lubricants

MDPI

Article

Influence of 3D-Printed PEEK on the Tribo-Corrosion Performance of Ti6Al4V Biomedical Alloy

Dominik Jonas Federl [1] and Abbas Al-Rjoub [1,2,3,*]

[1] Polymer-Tribology Group, Division of Machine Elements, Department of Engineering Sciences and Mathematics, Luleå University of Technology, Campus Porsön, 971 87 Luleå, Sweden; domi.federl@gmail.com
[2] TINT—Laboratory for Tribology and Interface Nanotechnology, Faculty of Mechanical Engineering, University of Ljubljana, Aškerčeva 6, 1000 Ljubljana, Slovenia
[3] Department of Mechanical Engineering, University of Coimbra, CEMMPRE, ARISE, Rua Luís Reis Santos, 3030-788 Coimbra, Portugal
* Correspondence: abbas.al-rjoubl@associated.ltu.se

Abstract

This study investigates the tribo-corrosion behavior of Ti6Al4V biomedical alloy, when sliding against fused filament fabrication (FFF) 3D-printed polyether ether ketone (PEEK) pins in a phosphate-buffered saline (PBS) solution. This research aims to evaluate wear mechanisms and electrochemical responses under simulated physiological conditions, providing critical insights for enhancing the durability and performance of biomedical implants. Potentiodynamic polarization tests demonstrate that the Ti6Al4V alloy possesses excellent corrosion resistance, which is further enhanced under sliding conditions compared to the test without sliding. When tested against 3D-printed PEEK, the alloy exhibits a mixed wear mechanism characterized by both abrasive and adhesive wear. Open-circuit potential (OCP) measurement of Ti6Al4V demonstrates the alloy's superior electrochemical stability, indicating high corrosion resistance and a favorable coefficient of friction. These findings highlight the potential of 3D-printed PEEK as a viable alternative for biomedical applications, offering rapid patient-specific prototyping, tunable mechanical properties, and improved surface adaptability compared to conventional materials.

Keywords: corrosion resistance; tribo-corrosion; friction; Ti6Al4V; 3D-printed PEEK

check for updates

Received: 17 May 2025
Revised: 12 June 2025
Accepted: 24 June 2025
Published: 25 June 2025

Citation: Federl, D.J.; Al-Rjoub, A. Influence of 3D-Printed PEEK on the Tribo-Corrosion Performance of Ti6Al4V Biomedical Alloy. *Lubricants* **2025**, *13*, 283. https://doi.org/10.3390/lubricants13070283

Copyright: © 2025 by the authors. Licensee MDPI, Basel, Switzerland. This article is an open access article distributed under the terms and conditions of the Creative Commons Attribution (CC BY) license (https://creativecommons.org/licenses/by/4.0/).

1. Introduction

Recent research indicates that 4.4% of 60,000 patients in the UK who underwent hip replacement surgery required revision surgery within the first 10 years, increasing up to 15% by the 20-year mark. Similarly, among nearly 55,000 individuals who had knee replacement surgery, 3.9% needed revision within 10 years, with the rate rising to 10.3% by 20 years [1]. As tribo-corrosion and osteolysis induced by wear particles are important factors in total joint replacement failure, there is a need for alternative materials with improved wear resistance in order to improve the survivorship of artificial hip joints in patients and reduce the amount of revision surgeries. Materials which feature advanced mechanical strength, mechanical reliability, and high wear and corrosion resistance while still maintaining biocompatibility must be considered [2].

Ultra-high-molecular-weight polyethylene (UHMWPE), polyether ether ketone (PEEK), and various other biomedical polymers in medical device engineering are critical materials in modern medical device design, each offering distinct advantages for specific clinical applications. For example, UHMWPE has long been considered as the gold-standard bearing

material in orthopedic implants and TJRs. Its outstanding wear resistance, low friction coefficient, high biocompatibility, and excellent impact toughness make it particularly well-suited for articulating surfaces, such as acetabular liners in hip replacements and tibial inserts in knee prostheses [3–5]. However, its relatively low elastic modulus (~0.5 GPa), propensity for wear debris generation, and susceptibility to gamma radiation-induced oxidation present significant limitations [4,6,7]. In contrast, PEEK's superior mechanical strength (elastic modulus ~3.6 GPa), excellent chemical resistance, and compatibility with multiple sterilization modalities make it particularly valuable for load-bearing applications such as spinal cages and trauma fixation devices, where its bone-like stiffness helps minimize stress shielding [8–10]. Despite these advantages, PEEK is more expensive than UHMWPE and lacks the ultra-low friction and wear resistance needed for joint articulation surfaces. Complementary polymers like Polymethylmethacrylate (PMMA) are mainly used as bone cement and in intraocular lenses, though they are inherently brittle and may release heat during polymerization [11], and polylactic and polyglycolic acids (PLA/PGA) are used in absorbable sutures and temporary fixation devices. These materials degrade via hydrolysis into biocompatible byproducts, although localized inflammatory responses can occur if degradation is not well-controlled [12].

On the other hand, metallic biomaterials are subjected to corrosion and tribo-corrosion degradation, which can lead to the release of metal ions. These ions may disrupt the optimal physiological balance of ions in neural cells, potentially causing adverse effects. As corrosion is dependent on gradients of metallic and electrolytic ion concentrations, temperature, ambient pressure, and the presence of other metals, bacteria, or active cells, the corrosion behavior of biomaterials must be examined meticulously. Moreover, the implant surfaces are subjected to load, impact, and wear [2,13–15].

Ti6Al4V is used in orthopedic implants due to its excellent strength-to-weight ratio, relatively low Young's modulus, and outstanding corrosion resistance. Additionally, it exhibits good biocompatibility, facilitated by the formation of a stable TiO_2 passive layer, along with good osteointegration and osteo-generation properties that promote strong bonding with bone tissue. This feature enhances implant integration, making Ti6Al4V a reliable choice for biomedical applications [2,16–18]. However, challenges remain, such as its stiffness mismatch and limitations in wear resistance and tribo-corrosion, particularly in dry and wet environments against articulating surfaces [16].

To address these issues, the combination of Ti-alloy and PEEK can present an attractive tribo-corrosion pair for hip implants due to their complementary properties. PEEK offers superior wear resistance, excellent chemical stability, and biocompatibility compared to Ti6Al4V, making it a valuable material for medical applications [19]. Its high strength-to-weight ratio and ability to withstand physiological conditions contribute to the durability of implants. When paired with Ti-alloy, this combination forms an optimized bearing system that minimizes friction, enhances scratch resistance, and reduces the generation of wear particles that are generally considered more harmful than PEEK particles, especially regarding inflammatory reactions and osteolysis. These characteristics collectively improve overall performance, making Ti6Al4V-PEEK an effective solution for long-lasting and reliable implants [16,17,20,21].

The key advantage of using 3D-printed PEEK over conventional injection-molded PEEK is its ability to fabricate complex freeform geometries without the constraints of traditional manufacturing methods. This technology offers superior design flexibility, allowing for the customization of components with tailored mechanical properties, as well as good surface adaptability. Additionally, metallic alloys exhibit improved electrochemical stability and tribological performance when tested against 3D-printed PEEK, making it highly suitable for wear-resistant biomedical applications. Unlike injection-molded PEEK, which

often leads to material waste, 3D-printing is an additive process that optimizes resource efficiency while minimizing waste. Moreover, it accelerates innovation by enabling rapid prototyping, testing, and design modifications without the need for costly molds, making it a highly attractive choice for advanced medical and engineering applications [22–24].

Therefore, the main objective of this research is to investigate the tribo-corrosion behavior of Ti6Al4V biomedical alloy when tested against 3D-printed PEEK pins in a phosphate-buffered saline (PBS) environment at room temperature.

2. Materials and Experimental Details

2.1. Materials

2.1.1. Polyetheretherketone (PEEK) Pins

Three-dimensionally printed (FFF) PEEK pins were used as the counter material in the tribo-corrosion tests. The filament materials were extruded from natural colored, high-viscosity PEEK resin. It is a testing-grade material designed for research, development, and process optimization. The dry properties of these pins, as provided by the supplier, are summarized in Table 1.

Table 1. Properties of the 3D-printed (FFF) PEEK.

	3D-Printed (FFF)
Tensile modulus [MPa]	3500
Yield stress [Mpa]	94
Yield strain [MPa]	5
Melting temperature [°C]	338
Glass transition temp. (DSC) [°C]	152
Density $\left[\mathrm{kg/m^3}\right]$	1300

2.1.2. Ti6V4Al

The Ti6Al4V material used in this study is an extra-low interstitials (ELI) grade 23 Ti6Al4V ELI, also known as ASTM F136 medical grade, supplied by S + D Metals, produced using the Electron Beam Melting (EBM) additive manufacturing technique in a high-vacuum atmosphere. The chemical composition of the alloy, as provided by the supplier, is detailed in Table 2. Compared to standard Grade 5 Ti6Al4V, this ELI variant exhibits significantly reduced impurity levels (e.g., nitrogen, oxygen, and carbon), enhancing its suitability for medical applications. It is designed specifically for medical and surgical implants, with improved biocompatibility, resistance to crack propagation, and enhanced fatigue strength. Additionally, the measured hardness of Ti6Al4V is 331 HV $\pm$ 3 HV, which falls within the expected range for this kind of alloy.

Table 2. Chemical composition limits in weight % of Ti6Al4V as provided in the data sheet of the supplier.

Element	**Atomic [Wt.%]**
Aluminum	5.50–6.50
Vanadium	3.50–4.50
Iron	Max. 0.25
Oxygen	Max. 0.13
Carbon	Max. 0.08
Titanium	Rest

2.1.3. Phosphate-Buffered Saline (PBS)

The water-based phosphate-buffered saline (PBS) solution from Merck supplier was used as the lubricating and corrosive medium in the tribo-corrosion tests. It comes in the form of tablets, consisting of 10 mM phosphate buffer and 3 mM KCl, with a pH of 7.4 at 25 °C. Dissolving one tablet in 1 L of deionized H_2O yields a solution containing 140 mM NaCl and 3 mM KCl, with a pH of 7.4 at 25 °C.

2.2. Preparation of Samples and Materials

The PEEK samples were fabricated via fused filament fabrication (FFF) in a horizontal build orientation, using a 1.75 mm diameter filament with a dimensional tolerance of ±0.02 mm and a printing speed of 20 mm/s. Pins with a size of 4 mm × 4 mm × 6 mm were then machined from the 3D-printed blocks for tribo-corrosion tests.

Ti6Al4V disks of 30 mm in diameter and 3 mm in thickness were machined from a larger bar using a lathe and subsequently polished to a surface roughness (Sa) of approximately 0.2 µm with SiC polishing paper (grit size 600). The disks were then ultrasonically cleaned in acetone for 15 min and ethanol for 10 min.

2.3. Design and Fabrication of the Corrosive Cell and Pin-Holder

Figure 1 shows the custom-designed cell and pin-holder used for the tribo-corrosion experiments. The components of the corrosive cell and pin-holder were designed and fabricated for the setup. The 3D models were created using CAD, NX 1899 software, and ideaMAKER, and were exported for fabrication. The components were 3D-printed with the Raise3D E2 model printer using 1.75 mm Polylactide filament. For the tribo-corrosion cell, the selected infill percentage was 10%, while for the pin-holder, a higher infill of 75% was used.

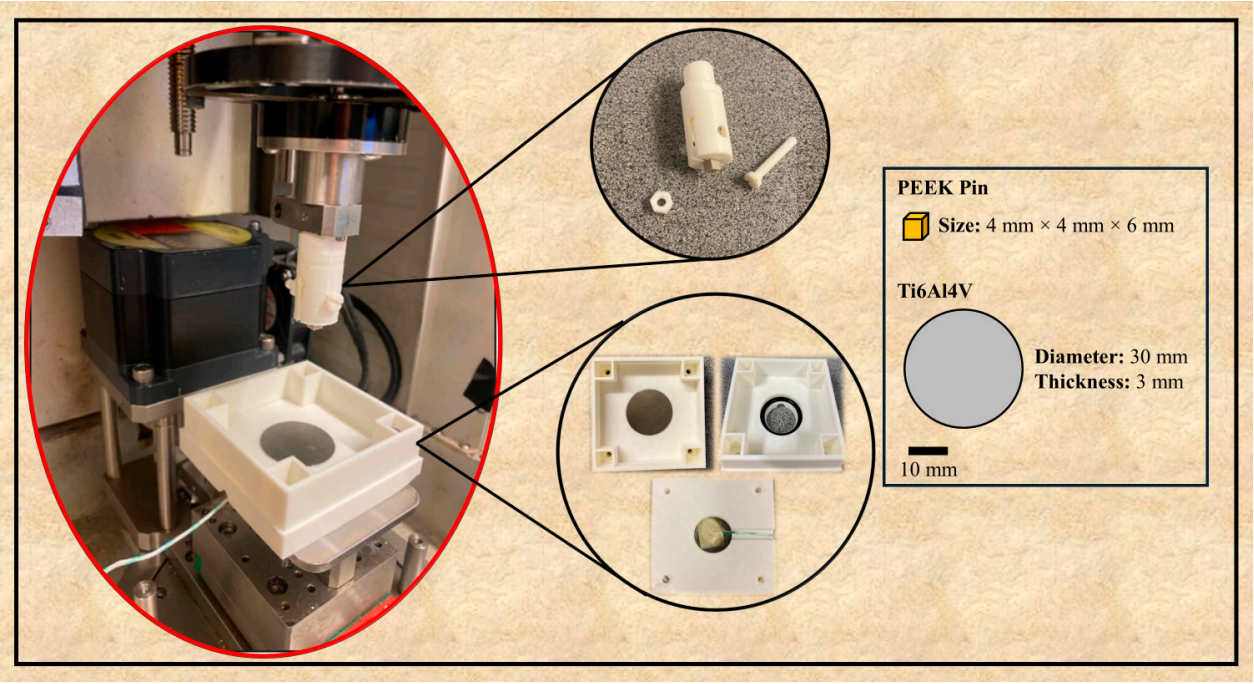


Figure 1. The custom-designed corrosive cell and pin-holder used for tribo-corrosion experiments, showing the PEEK pin and Ti6Al4V alloy with their respective dimensions.

2.4. Corrosion and Tribo-Corrosion Tests

The setup for the corrosion (without and during sliding) and tribo-corrosion tests is presented in Figure 2. For the electrochemical corrosion without sliding, the same cell

was used without the pin-holder. A three-electrode cell configuration was used, where the electrodes are in contact with the corrosive PBS electrolyte, and the surface of the sample was horizontally positioned. The Ti6Al4V disk served as the working electrode, a platinum wire electrode was used as the counter electrode, and a Silver/Silver Chloride (Ag/AgCl) electrode was used as the reference electrode. The Ag/AgCl electrode has a potential of 0.199 Volt versus the standard hydrogen electrode when saturated in potassium chloride (KCl), and 242 mV versus the standard hydrogen electrode for the Saturated Calomel Electrode (SCE). The exposed surface area of the sample was approximately 7.065 cm^2. The corrosion measurements, open-circuit potential (OCP), and electrochemical polarization were performed at room temperature in 60 mL of PBS salt solution of electrolyte using a potentiostat Autolab PGSTAT302 Echochemie (Metrohm, Herisau, Switzerland). The electrochemical activity was stabilized for 30 min to reach a stable OCP, and then a potentiodynamic polarization test was carried out at a rate of 0.6 mv/s starting at −1.5 V below the OCP up to a maximum of 1 V above the OCP.

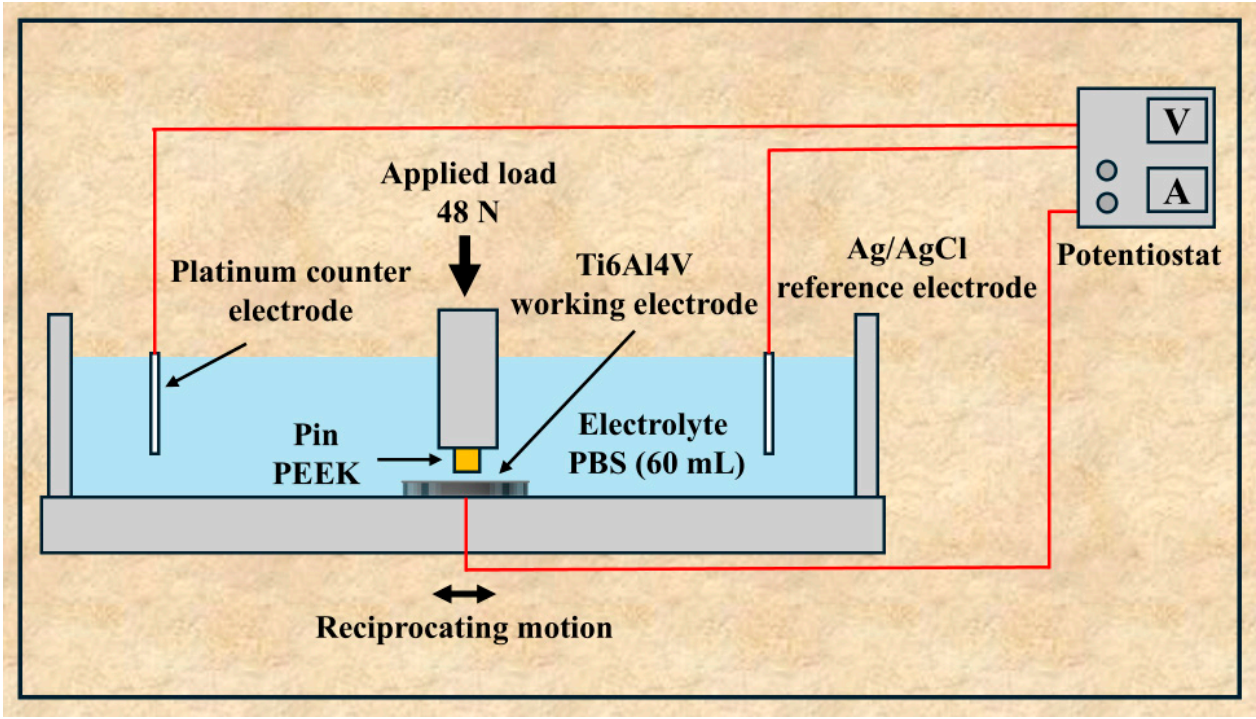


Figure 2. Schematic setup of corrosion and tribo-corrosion cell.

For tribo-corrosion tests, a UMT-2 tribometer (Bruker, Billerica, MA, USA) was used in a reciprocating pin-on-disk configuration to evaluate the tribo-corrosion behavior of Ti6Al4V against the 3D-printed PEEK pins. The tests were performed under OCP in PBS solution with a normal load of 48 N corresponding to ~ 3.0 MPa contact pressure, a frequency of the reciprocating motion of 1 Hz, and a total stroke length of 6 mm for 2 h. The tribo-corrosion behavior was investigated through the evolution of the OCP curve as a function of time before (30 min), during (120 min), and after the wear test (30 min). The coefficient of friction (COF) was continuously acquired during the tests. The tests were repeated three times, and the average values with standard deviation errors are presented in this study.

2.5. Characterization

The microhardness of Ti6V4Al was evaluated using a Matsuzawa MXT-alpha, Matsuzawa, Japan (Chennai Metco, Chennai, India), with a Vickers diamond tip. A load of

300 g-force was applied for 15 s. The tests were repeated six times, and the average values with standard deviation errors were calculated.

The surface topography measurements, especially the roughness (S_a) of the polymer pins and Ti6Al4V counter faces, were conducted using a Zygo NewView 9000 optical (Zygo, Middlefield, CT, USA) profilometer.

Infrared spectroscopy analysis was performed using a Fourier Transform Infrared Spectroscopy (FTIR) Nicolet 380 (LabX, Midland, ON, Canada) spectrometer with the built-in diamond ATR. The spectra were collected in the wavelength from 3200 cm^{-1} to 400 cm^{-1} with a resolution of 2 cm^{-1}.

The chemical composition and surface morphology of Ti6AlV4 disks before and after each test were studied by a JEOL JCM-6000 (Excel Technologies (Inc.), Enfield, CT, USA), equipped with an energy-dispersive X-ray spectrum (EDS). The EDS measurements were conducted applying an acceleration voltage of 15 keV.

3. Results and Discussion

3.1. Surface Morphology of PEEK Pins and Ti6Al4V Alloy

Figure 3 presents the surface morphology of the 3D-printed PEEK pins and Ti6Al4V disk prior to tribological testing, as characterized by optical profilometry. The PEEK surface exhibits randomly distributed scratches, yielding an average arithmetic mean roughness (Sa) of 0.49 µm. In contrast, the Ti6Al4V disk was mechanically polished to a smoother finish (Sa = 0.21 µm) to replicate the surface conditions typical of biomedical implants, as established in prior studies [22,25]. This polishing process produced unidirectional parallel scratches on the Ti6Al4V surface, consistent with standard metallographic preparation techniques for tribo-corrosion testing. The controlled surface finish of both materials ensures comparability with clinical implant performance metrics while minimizing initial roughness effects on wear behavior.

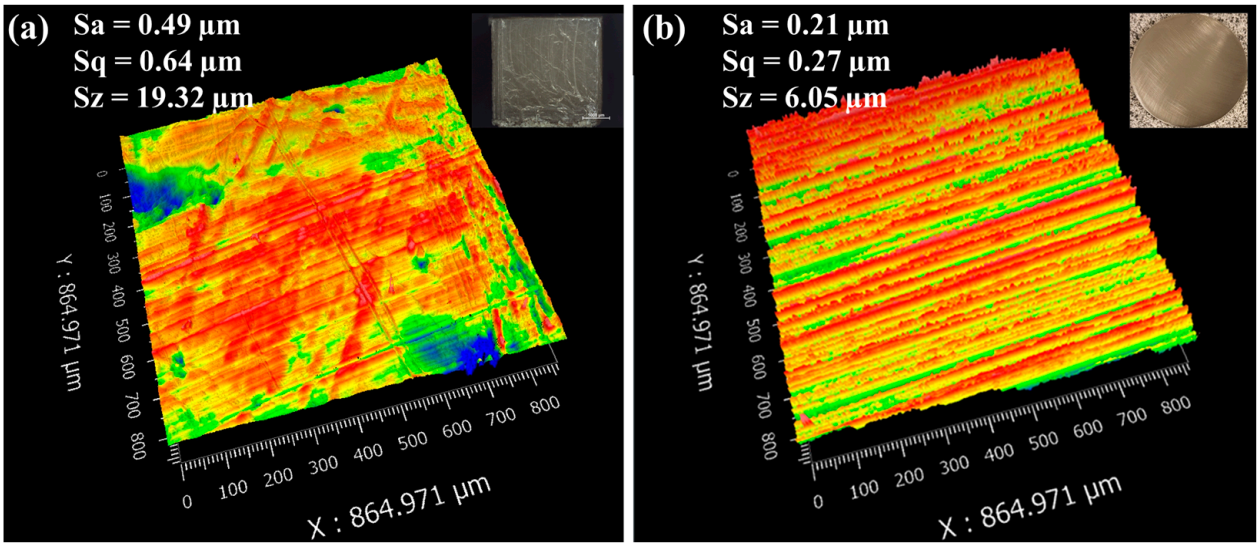


Figure 3. Morphological surfaces images of (**a**) 3D-printed PEEK and (**b**) Ti6Al4V before tribo-corrosion tests, obtained by an optical profilometer.

3.2. Corrosion Resistance of Ti6Al4V Alloy

The potentiodynamic polarization curves for the Ti6Al4V alloy substrate in PBS solution, with and without sliding, are shown in Figure 4, while their corresponding corrosion parameters are presented in Table 3. The curves (Figure 4a) demonstrate the relationship between current density and the changing potential of the working electrode,

showing passive behavior due to the formation of a protective oxide layer. As shown in Figure 4b,c, no local corrosive damages such as pits and cracks were detected after both corrosive polarization tests, reflecting the high corrosion resistance of the Ti6Al4V alloy.

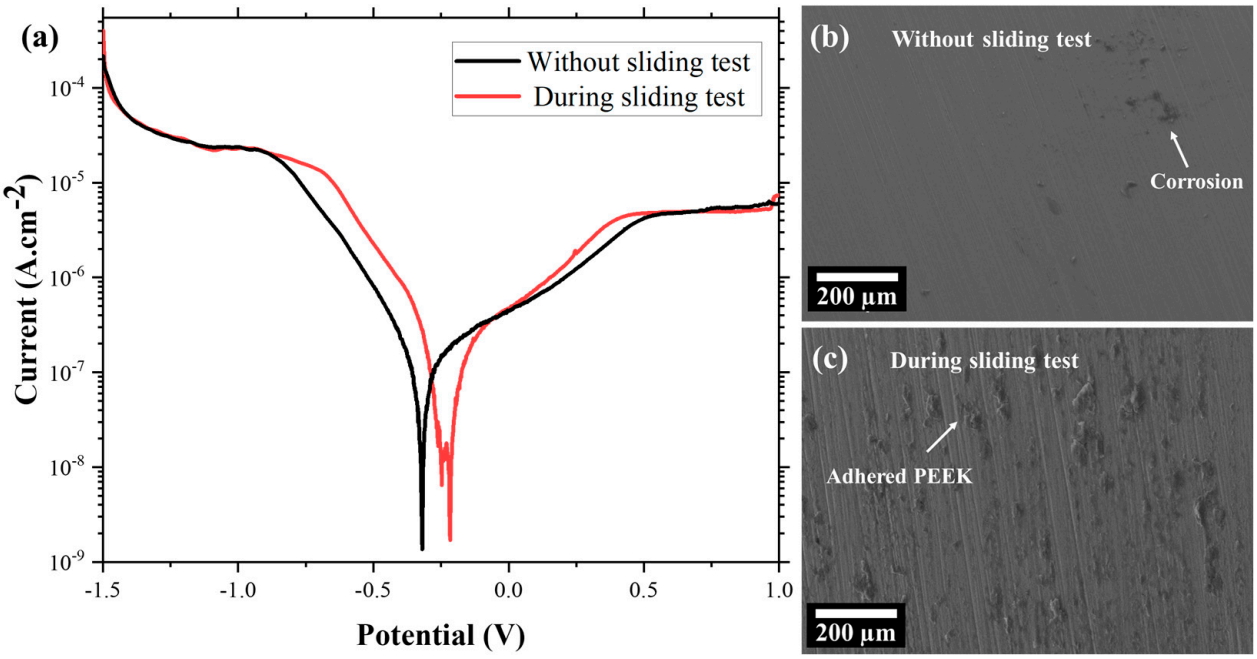


Figure 4. (**a**) Potentiodynamic polarization curve of the Ti6Al4V alloy substrate in PBS solution, along with top-surface SEM images of the Ti6Al4V sample after corrosion testing (**b**) without sliding and (**c**) during sliding against PEEK pins.

Table 3. Corrosion proprieties and parameters of Ti6Al4V alloy obtained from the polarization curves of without sliding and during sliding against PEEK Pins.

Element	Without Sliding	During Sliding
i_{corr} ($\mu A/cm^2$)	15.59 ± 0.03	13.27 ± 0.04
E_{corr} (V)	−0.32 ± 0.02	−0.22 ± 0.03
Polarization resistance (Ω)	69,477 ± 3100	67,866 ± 310
Corrosion Rate (mm/Year)	0.059 ± 0.004	0.051 ± 0.005

In the case of the test without sliding, the polarization curve reveals exceptionally low values for corrosive current density (I_{corr} = 15.59 $\mu A/cm^2$), corrosive potential (E_{corr} = −0.32 V), and corrosion rate (0.059 mm/year), indicating outstanding corrosion resistance in PBS solutions. Moreover, the SEM image (Figure 4b) further supports the high corrosion resistance of the sample where no corrosive signs were reported. These findings are consistent with those reported by Manhabosco et al. [23], who investigated the corrosion resistance of bare and nitrided Ti6Al4V alloy in PBS solution.

On the other hand, the corrosion resistance of the Ti6Al4V is clearly affected by sliding, as evidenced by both electrochemical data and surface morphology. During sliding, the V–I curve shows small fluctuation with corrosive current density, decreasing from 15.59 to 13.27 $\mu A/cm^2$, and the corrosive potential (E_{corr}) shifted from −0.32 V to a lower negative value of −0.22 V compared with tests without sliding, indicating a lower tendency for corrosion. Additionally, the corrosion rate decreased from 0.059 to 0.051 mm/year, reflecting a 13.6% decrease in Ti6Al4V degradation under sliding conditions. Interestingly, the polarization resistance showed a slight decrease, which may be attributed to dynamic

oxide layer formation or localized electrochemical effects. Surface images support these findings: the surfaces of samples without sliding appear smooth and uniform, while those during sliding reveal a distinct wear track, with pronounced abrasive grooves parallel to the sliding direction and debris adhered onto the middle of the wear track. This reveals that adhered PEEK debris can protect the Ti6Al4V alloy against further corrosion. Overall, these results confirm that sliding slows corrosion.

3.3. Evolution of the Open-Circuit Potential (OCP) and Coefficient of Friction (COF)

The evolution of the OCP over time, before, during, and after the tribo-corrosion reciprocating sliding test on Ti6Al4V alloy, tested against 3D-printed PEEK pins in PBS solution, is shown in Figure 5a. The potential of all samples was stabilized for 30 min before and after sliding tests, to ensure that all electrochemical activities including oxidation and reduction reactions on the surface were in equilibrium. This OCP behavior is a typical characteristic observed in tribo-corrosion studies [26]. Before the sliding test, with no load applied, the OCP for the Ti6Al4V alloy stabilized at approximately −0.35 V, indicating the formation of a passive thin oxide layer on the surface [27]. Upon applying the load and initiating reciprocating sliding, a sharp decrease in OCP values, accompanied by fluctuations, was observed, suggesting partial removal of the protective oxide layer [28]. However, after 4000 s, the OCP values gradually increased due to the transfer and adhesion of PEEK material onto the Ti6Al4V surface, forming a protective barrier that enhanced corrosion resistance as reported [19].

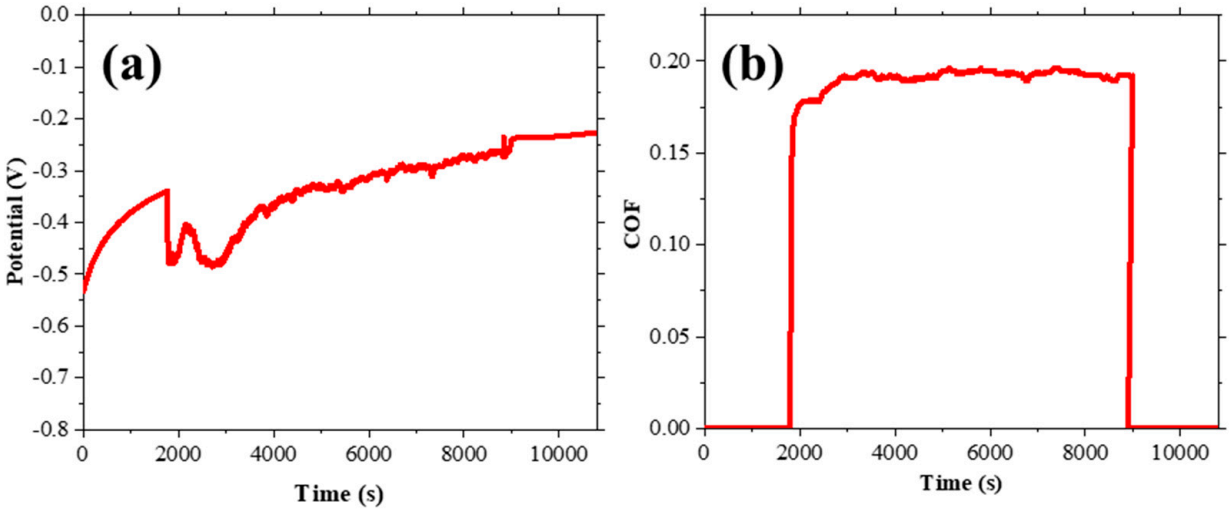


Figure 5. (**a**) OCP as a function of time before, during, and after the tribo-corrosion reciprocating sliding test conducted on Ti6Al4V alloy against 3D-printed pins in PBS solution, with (**b**) corresponding to COF.

After 9000 s of sliding, once the load was removed and the test completed, the OCP values increased, indicating a good re-passivation of the Ti6Al4V surface and good electrochemical stability, suggesting high corrosion resistance.

The initial increase in the COF corresponds to a noticeable decline in the OCP values, which is a typical behavior of the tribo-corrosion test [29]. Specifically, the COF shows a marked increase during the sliding test. The COF values did not show a significant running-in phase and instead maintained a stable steady-state COF (0.19) throughout the duration of the test, suggesting that the PBS solution functions effectively as a lubricant in both cases. The absence of a running-in phase can be attributed to the significantly low surface roughness of the polymer pins and Ti6Al4V alloy, as discussed earlier.

To better understand the friction and wear behaviors described above, a detailed analysis of the wear mechanisms, including characterization of the wear tracks and debris, is conducted. Figure 6 displays typical wear track micrographs of Ti6Al4V samples after the tribo-corrosion reciprocating sliding test conducted on Ti6Al4V alloy against 3D-printed pins in PBS solution, along with the corresponding EDS spectra of chosen areas in the wear tracks.

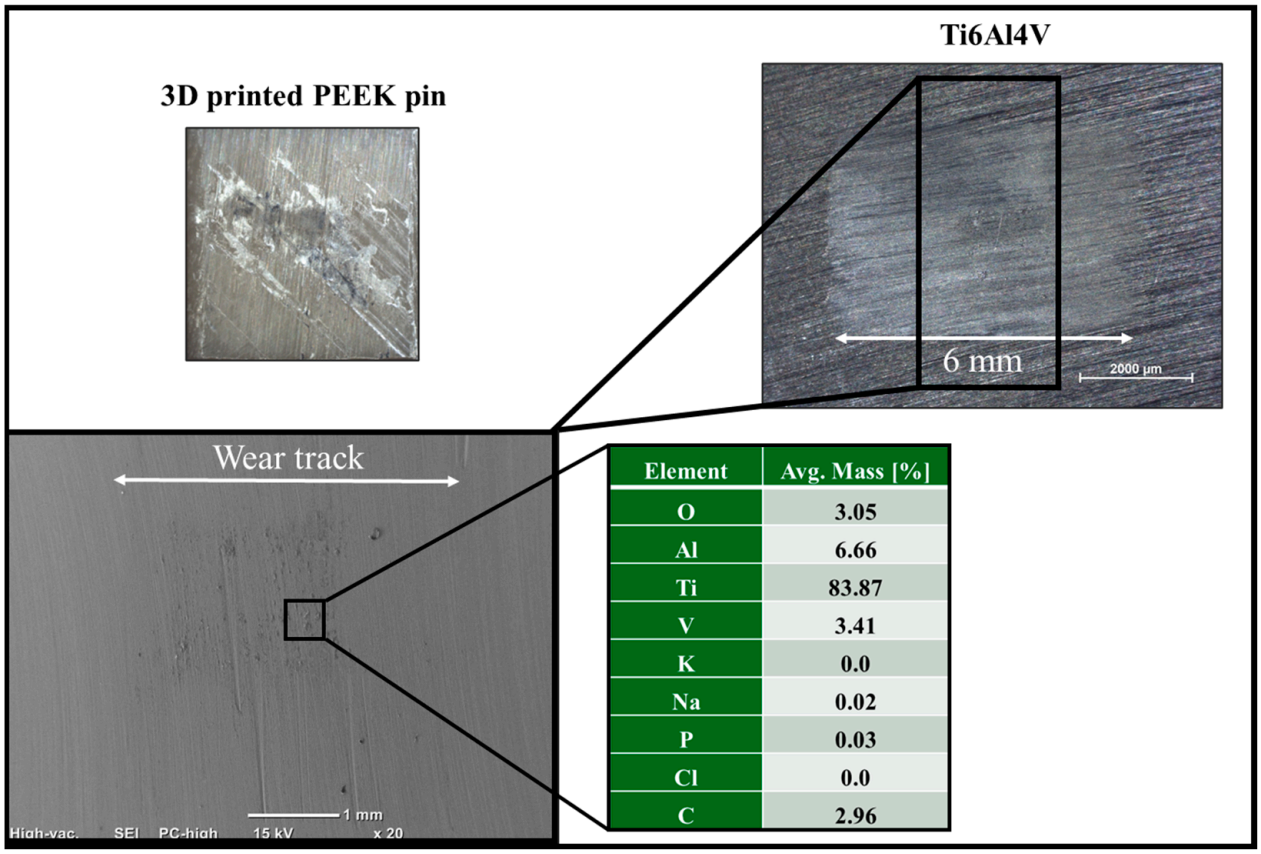


Figure 6. Wear track micrographs of Ti6Al4V samples after tribo-corrosion against 3D-printed PEEK ins in PBS solution, with the corresponding EDS spectra of a chosen area in the wear tracks.

The average specific wear volume of the PEEK pins, calculated from mass loss after sliding tests, is approximately $(8.1 \pm 1.2) \times 10^{-4}$ mm^3/N·m. In contrast, the specific wear volume of the Ti6Al4V disks could not be measured from the wear track profiles. To further investigate the wear mechanisms of Ti6Al4V disks, SEM imaging and FTIR analysis were employed. Considering that the tribological tests were performed in corrosive salt solutions, the wear track of the surface tested against the PEEK pins exhibited a wear mechanism characterized by both abrasive and adhesive wear debris. Its surfaces show pronounced abrasive grooves parallel to the sliding direction, with debris adhered onto the middle of the wear track, indicating a combination of severe abrasive and adhesive wear. EDS analysis of the chosen wear area reveals a mixture of elements from the Ti6Al4V disks and salt components of the PBS corrosive solution, which is consistent with findings reported in previous studies on corrosion and tribo-corrosion in PBS solution [30,31]. To assess whether the salts in PBS significantly affect the oxidation resistance of Ti6Al4V, the alloy was immersed in PBS for 3 h (without sliding) and analyzed via FTIR (Figure 7). Only very weak metal oxide peaks were detected, confirming the alloy's high oxidation resistance. The slight increase in oxygen content observed after tribo-corrosion testing is likely attributable to oxide formation from salt constituents and minor localized corrosion,

as corroborated by FTIR analysis (Figure 7), where the adsorption bands corresponding to alloy surface groups shown at 1400–1500 cm^{-1} and 871 cm^{-1} indicate stretching vibrations of CO_3^{2-}, and adsorption bands of metal oxides and metal-OH bonds on alloys surface appear at 1100–450 cm^{-1} [15]. These findings, along with the absence of macroparticles, defects, or pinholes on the surfaces, further confirm the alloy's high corrosion resistance.

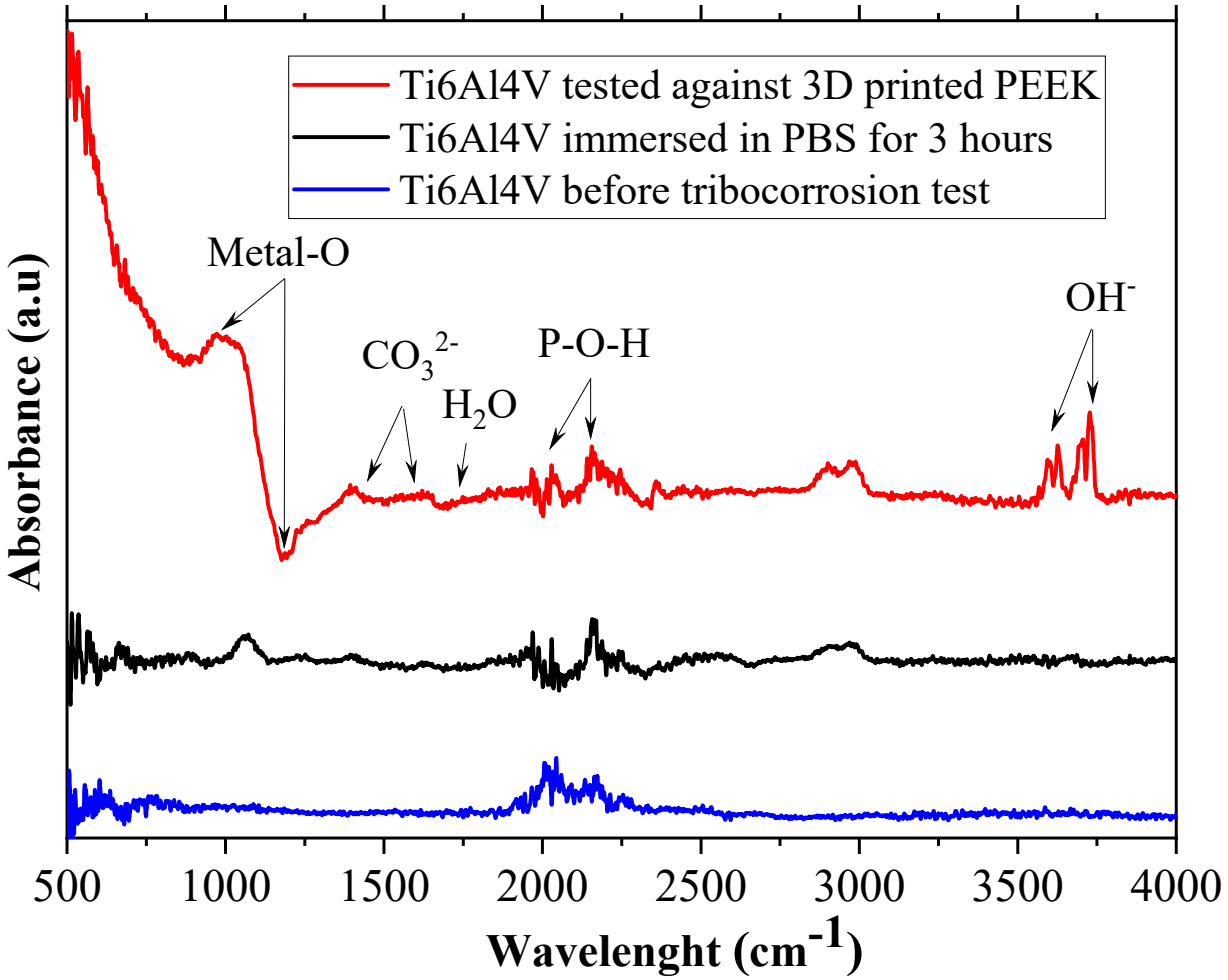


Figure 7. FTIR spectra of Ti6Al4V surfaces before and after tribo-corrosion tests, and after immersion in PBS for 3 h.

4. Conclusions

This study offers valuable insights into the corrosion resistance of Ti6Al4V under both static and sliding conditions against 3D-printed (FFF) PEEK, as well as its tribo-corrosion behavior in a phosphate-buffered saline (PBS) solution at room temperature. Surface morphology analysis revealed that 3D-printed PEEK exhibits significantly low roughness, influencing its tribological performance. Potentiodynamic polarization tests demonstrate that the Ti6Al4V alloy possesses excellent corrosion resistance, which is further enhanced under sliding conditions compared to the test without sliding. The OCP of Ti6Al4V revealed that the alloy shows high corrosion resistance and stability by promoting superior re-passivation. Also, it exhibited a coefficient of friction of 0.19. Wear track analysis confirmed that the PEEK pins induced a combination of abrasive and adhesive wear on Ti6Al4V, with EDS and FTIR results confirming the formation of protective oxide layers. The findings highlight the potential of 3D-printed PEEK as a promising alternative for biomedical applications, offering superior surface adaptability, enhanced corrosion resistance of Ti6Al4V, and great design flexibility.

Author Contributions: Conceptualization, D.J.F. and A.A.-R.; Validation, D.J.F. and A.A.-R.; Formal analysis, D.J.F.; Investigation, D.J.F. and A.A.-R.; Writing—original draft, D.J.F. and A.A.-R.; Writing—review & editing, A.A.-R.; Visualization, A.A.-R.; Supervision, A.A.-R.; Project administration, A.A.-R.; Funding acquisition, A.A.-R. All authors have read and agreed to the published version of the manuscript.

Funding: This research was funded by Slovenian Research Agency ARIS under the Research Core Funding Programme No. P2-0231 and Marie-Sklodowska Curie COFUND—Seal of Excellence No. 5100-237/2023-7 (5 February 2024).

Data Availability Statement: Data is contained within the article.

Acknowledgments: The authors acknowledge Nazanin Emami for her invaluable guidance, insightful suggestions, and dedicated supervision throughout this work. Also, they acknowledge the support of Laboratory for Polymer-Tribology Group, Division of Machine Elements, Department of Engineering Sciences and Mathematics, Luleå University of Technology.

Conflicts of Interest: The authors declare no conflict of interest.

References

1. Bayliss, L.E.; Culliford, D.; Monk, A.P.; Glyn-Jones, S.; Prieto-Alhambra, D.; Judge, A.; Cooper, C.; Carr, A.J.; Arden, N.K.; Beard, D.J.; et al. The effect of patient age at intervention on risk of implant revision after total replacement of the hip or knee: A population-based cohort study. *Lancet* **2017**, *389*, 1424–1430. [CrossRef]
2. Hu, C.Y.; Yoon, T.R. Recent updates for biomaterials used in total hip arthroplasty. *Biomater. Res.* **2018**, *22*, 33. [CrossRef] [PubMed]
3. Lewis, G. Properties of crosslinked ultra-high-molecular-weight polyethylene. *Biomaterials* **2001**, *22*, 371–401. [CrossRef] [PubMed]
4. Lapcikova, M.; Slouf, M.; Dybal, J.; Zolotarevova, E.; Entlicher, G.; Pokorny, D.; Gallo, J.; Sosna, A. Nanometer size wear debris generated from ultra high molecular weight polyethylene in vivo. *Wear* **2009**, *266*, 349–355. [CrossRef]
5. Patil, N.A.; Njuguna, J.; Kandasubramanian, B. UHMWPE for biomedical applications: Performance and functionalization. *Eur. Polym. J.* **2020**, *125*, 109529. [CrossRef]
6. Tipper, J.L.; Hailey, J.L.; Besong, A.A.; Fisher, J.; Wroblewski, B.M.; Stone, M.H. Quantitative analysis of polyethylene wear debris, wear rate and head damage in retrieved Charnley hip prostheses. *J. Mater. Sci. Mater. Med.* **2000**, *11*, 117–124. [CrossRef]
7. Premnath, V.; Harris, W.H.; Jasty, M.; Merrill, E.W. Gamma sterilization of UHMWPE articular implants: An analysis of the oxidation problem. *Biomoterials* **1996**, *17*, 1741–1753. [CrossRef] [PubMed]
8. Toth, J.M.; Wang, M.; Estes, B.T.; Scifert, J.L.; Seim, H.B.; Turner, A.S. Polyetheretherketone as a biomaterial for spinal applications. *Biomaterials* **2006**, *27*, 324–334. [CrossRef]
9. Katzer, A.; Marquardt, H.; Westendorf, J.; Wening, J.V.; Von Foerster, G. Polyetheretherketone-cytotoxicity and mutagenicity in vitro. *Biomaterials* **2002**, *23*, 1749–1759. [CrossRef]
10. Abu Bakar, M.S.A.; Cheng, M.H.W.; Tang, S.M.; Yu, S.C.; Liao, K.; Tan, C.T.; Khor, K.A.; Cheang, P. Tensile properties, tension-tension fatigue and biological response of polyetheretherketone-hydroxyapatite composites for load-bearing orthopedic implants. *Biomaterials* **2003**, *24*, 2245–2250. [CrossRef]
11. Xu, T.G.; Shi, J.; Qi, H.; Chen, S.; Li, B.; Zhang, F.; He, J.H. Radiopaque and Biocompatible PMMA Bone Cement Triggered by Nano Tantalum Carbide and Its Osteogenic Performance. *ACS Biomater. Sci. Eng.* **2024**, *10*, 5624–5631. [CrossRef] [PubMed]
12. Elmowafy, E.M.; Tiboni, M.; Soliman, M.E. Biocompatibility, biodegradation and biomedical applications of poly(lactic acid)/poly(lactic-co-glycolic acid) micro and nanoparticles. *J. Pharm. Investig.* **2019**, *49*, 347–380. [CrossRef]
13. Hodgson, A.W.E.; Kurz, S.; Virtanen, S.; Fervel, V.; Olsson, C.O.A.; Mischler, S. Passive and transpassive behaviour of CoCrMo in simulated biological solutions. *Electrochim. Acta* **2004**, *49*, 2167–2178. [CrossRef]
14. Bryant, M.; Neville, A. Fretting corrosion of CoCr alloy: Effect of load and displacement on the degradation mechanisms. *Proc. Inst. Mech. Eng. H* **2017**, *231*, 114–126. [CrossRef] [PubMed]
15. Pylypchuk, I.V.; Petranovskaya, A.L.; Gorbyk, P.P.; Korduban, A.M.; Markovsky, P.E.; Ivasishin, O.M. Biomimetic Hydroxyapatite Growth on Functionalized Surfaces of Ti-6Al-4V and Ti-Zr-Nb Alloys. *Nanoscale Res. Lett.* **2015**, *10*, 338. [CrossRef]
16. Bartolomeu, F.; Abreu, C.S.; Moura, C.G.; Costa, M.M.; Alves, N.; Silva, F.S.; Miranda, G. Ti6Al4V-PEEK multi-material structures–Design, fabrication and tribological characterization focused on orthopedic implants. *Tribol. Int.* **2019**, *131*, 672–678. [CrossRef]
17. Bartolomeu, F.; Buciumeanu, M.; Costa, M.M.; Alves, N.; Gasik, M.; Silva, F.S.; Miranda, G. Multi-material Ti6Al4V & PEEK cellular structures produced by Selective Laser Melting and Hot Pressing: A tribocorrosion study targeting orthopedic applications. *J. Mech. Behav. Biomed. Mater.* **2019**, *89*, 54–64. [CrossRef]

18. Buciumeanu, M.; Almeida, S.; Bartolomeu, F.; Costa, M.M.; Alves, N.; Silva, F.S.; Miranda, G. Ti6Al4V cellular structures impregnated with biomedical PEEK—New material design for improved tribological behavior. *Tribol. Int.* **2018**, *119*, 157–164. [CrossRef]
19. Sampaio, M.; Buciumeanu, M.; Henriques, B.; Silva, F.S.; Souza, J.C.M.; Gomes, J.R. Tribocorrosion behavior of veneering biomedical PEEK to Ti6Al4V structures. *J. Mech. Behav. Biomed. Mater.* **2016**, *54*, 123–130. [CrossRef]
20. Grieco, P.W.; Pascal, S.; Newman, J.M.; Shah, N.V.; Stroud, S.G.; Sheth, N.P.; Maheshwari, A.V. New alternate bearing surfaces in total hip arthroplasty: A review of the current literature. *J. Clin. Orthop. Trauma* **2018**, *9*, 7–16. [CrossRef]
21. Holzwarth, U.; Cotogno, G. *Total Hip Arthroplasty: State of the Art, Challenges and Prospects*; Publications Office: Luxembourg, 2012. [CrossRef]
22. Mani, G.; Feldman, M.D.; Oh, S.; Agrawal, C.M. Surface modification of cobalt-chromium-tungsten-nickel alloy using octadecyltrichlorosilanes. *Appl. Surf. Sci.* **2009**, *255*, 5961–5970. [CrossRef]
23. Manhabosco, T.M.; Tamborim, S.M.; dos Santos, C.B.; Müller, I.L. Tribological, electrochemical and tribo-electrochemical characterization of bare and nitrided Ti6Al4V in simulated body fluid solution. *Corros. Sci.* **2011**, *53*, 1786–1793. [CrossRef]
24. Honigmann, P.; Sharma, N.; Okolo, B.; Popp, U.; Msallem, B.; Thieringer, F.M. Patient-specific surgical implants made of 3D printed PEEK: Material, technology, and scope of surgical application. *Biomed. Res. Int.* **2018**, *2018*, 4520636. [CrossRef]
25. Chen, Q.; Thouas, G.A. Metallic implant biomaterials. *Mater. Sci. Eng. R Rep.* **2015**, *87*, 1–57. [CrossRef]
26. Buciumeanu, M.; Araujo, A.; Carvalho, O.; Miranda, G.; Souza, J.C.M.; Silva, F.S.; Henriques, B. Study of the tribocorrosion behaviour of Ti6Al4V–HA biocomposites. *Tribol. Int.* **2017**, *107*, 77–84. [CrossRef]
27. Totolin, V.; Pejaković, V.; Csanyi, T.; Hekele, O.; Huber, M.; Rodríguez Ripoll, M. Surface engineering of Ti6Al4V surfaces for enhanced tribocorrosion performance in artificial seawater. *Mater. Des.* **2016**, *104*, 10–18. [CrossRef]
28. Diomidis, N.; Mischler, S.; More, N.S.; Roy, M. Tribo-electrochemical characterization of metallic biomaterials for total joint replacement. *Acta Biomater.* **2012**, *8*, 852–859. [CrossRef]
29. Buciumeanu, M.; Bagheri, A.; Souza, J.C.M.; Silva, F.S.; Henriques, B. Tribocorrosion behavior of hot pressed CoCrMo alloys in artificial saliva. *Tribol. Int.* **2016**, *97*, 423–430. [CrossRef]
30. Feyzi, M.; Fallahnezhad, K.; Taylor, M.; Hashemi, R. What role do normal force and frequency play in the tribocorrosion behaviour of Ti-6Al-4 V alloy? *Tribol. Int.* **2022**, *172*, 107634. [CrossRef]
31. Hammood, A.S.; Thair, L.; Altawaly, H.D.; Parvin, N. Tribocorrosion Behaviour of Ti–6Al–4V Alloy in Biomedical Implants: Effects of Applied Load and Surface Roughness on Material Degradation. *J. Bio Tribo-Corros.* **2019**, *5*, 85. [CrossRef]

Disclaimer/Publisher's Note: The statements, opinions and data contained in all publications are solely those of the individual author(s) and contributor(s) and not of MDPI and/or the editor(s). MDPI and/or the editor(s) disclaim responsibility for any injury to people or property resulting from any ideas, methods, instructions or products referred to in the content.